The American Journal of Human Genetics, Volume *103*

Supplemental Data

Mutations in *LNPK*, Encoding the Endoplasmic Reticulum Junction Stabilizer Lunapark, Cause a Recessive Neurodevelopmental Syndrome

Martin W. Breuss, An Nguyen, Qiong Song, Thai Nguyen, Valentina Stanley, Kiely N. James, Damir Musaev, Guoliang Chai, Sara A. Wirth, Paula Anzenberg, Renee D. George, Anide Johansen, Shaila Ali, Muhammad Zia-ur-Rehman, Tipu Sultan, Maha S. Zaki, and Joseph G. Gleeson

Supplemental Figures and Tables

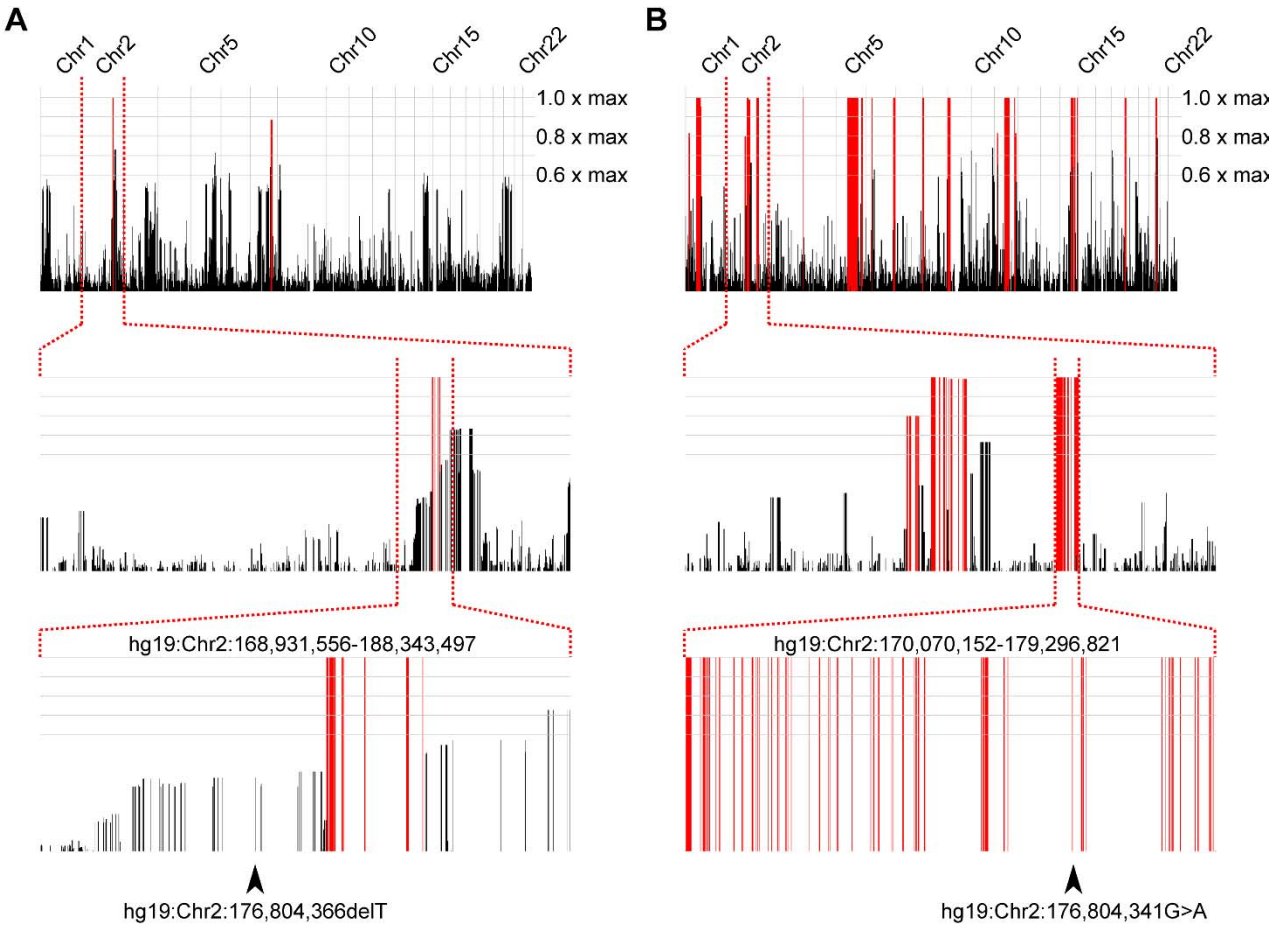

Figure S1. Homozygosity plots for families A and B.

(A-B) Graphical representation of the homzygosity plots generated by HomozygosityMapper for all 22 autosomes for the affected individuals in Family A (A) and B (B). Red peaks indicate homozygosity scores above the cutoff at 0.8x of the maximum. There is an extensive stretch of homozygosity on chromosome 2. Arrowheads in the lowest panel indicate the positions of the mutations. While the mutation in Family A lies just outside the significant stretch of homozygosity, manual inspection of the area revealed that sites contributing negatively to the score were generally of low quality, suggesting that the mutation most likely lies within this stretch of extended homozygosity.

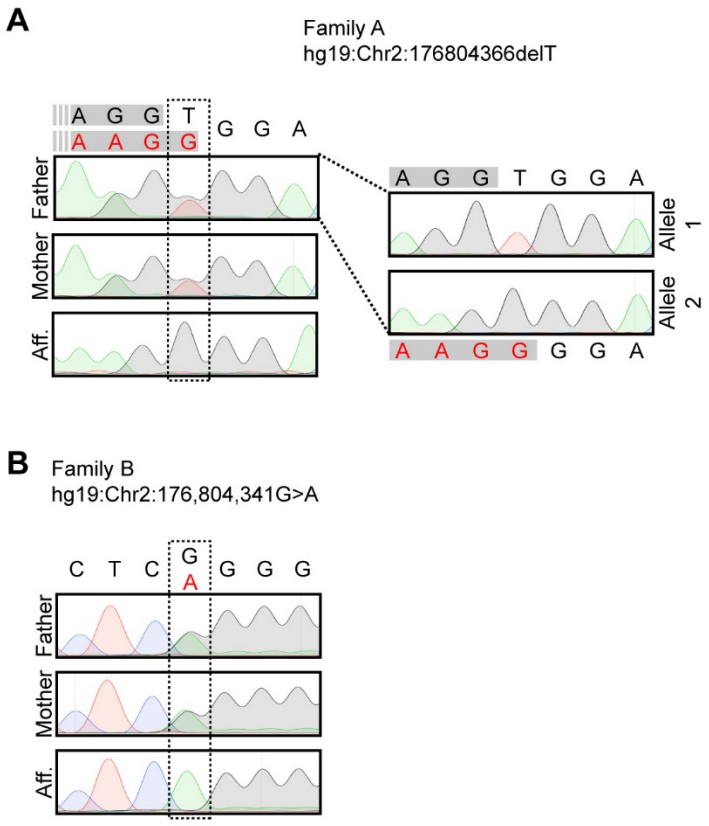

Figure S2. Sanger sequencing traces for families A and B.

(A) Sanger sequencing traces depicting the T deletion present in Family A that results in the frameshift mutation. For better clarity the two heterozygous alleles from the father are shown separated as well. Shown are traces for father, mother, and one of the two affected boys (Aff.); as expected from WES analysis, both parents are heterozygous and the affected child is homozygous for the mutation.

(B) Sanger sequencing traces depicting the G>A conversion present in Family B that results in the premature stop codon. Shown are traces for father, mother, and the affected girl (Aff.); as expected from WES analysis, both parents are heterozygous and the affected child is homozygous for the mutation.

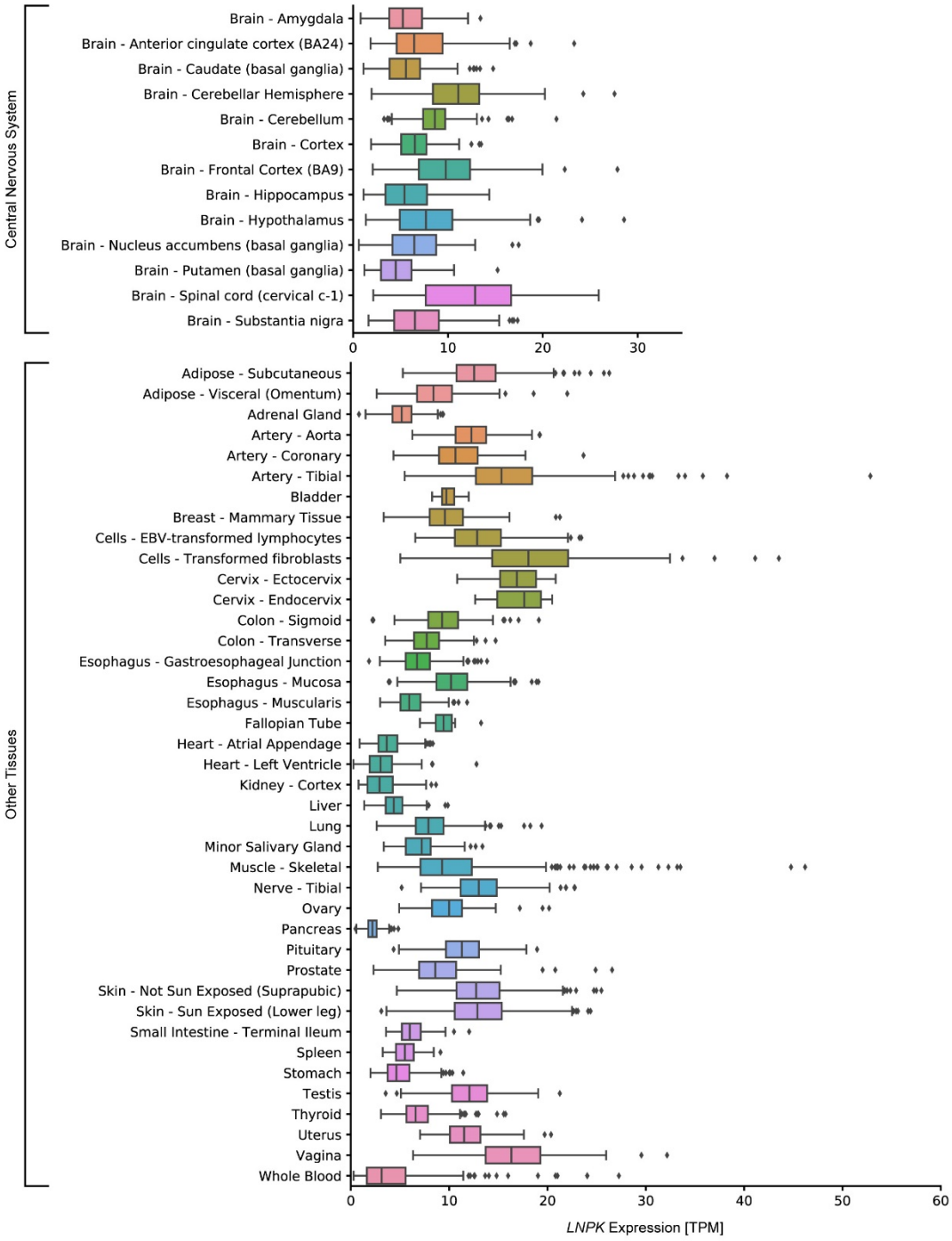

Figure S3. *LNPK* expression across various tissues in adult humans (GTEx data).

Expression analysis of *LNPK* transcripts across various adult tissues. Data is split into expression in the central nervous tissue and other tissues. *LNPK* shows ubiquitous expression

across all tissues. Expression is shown as Transcripts per Kilobase Million (TPM). Data used was derived from the GTEx portal.[33; 34] Shown are standard boxplots with outliers.

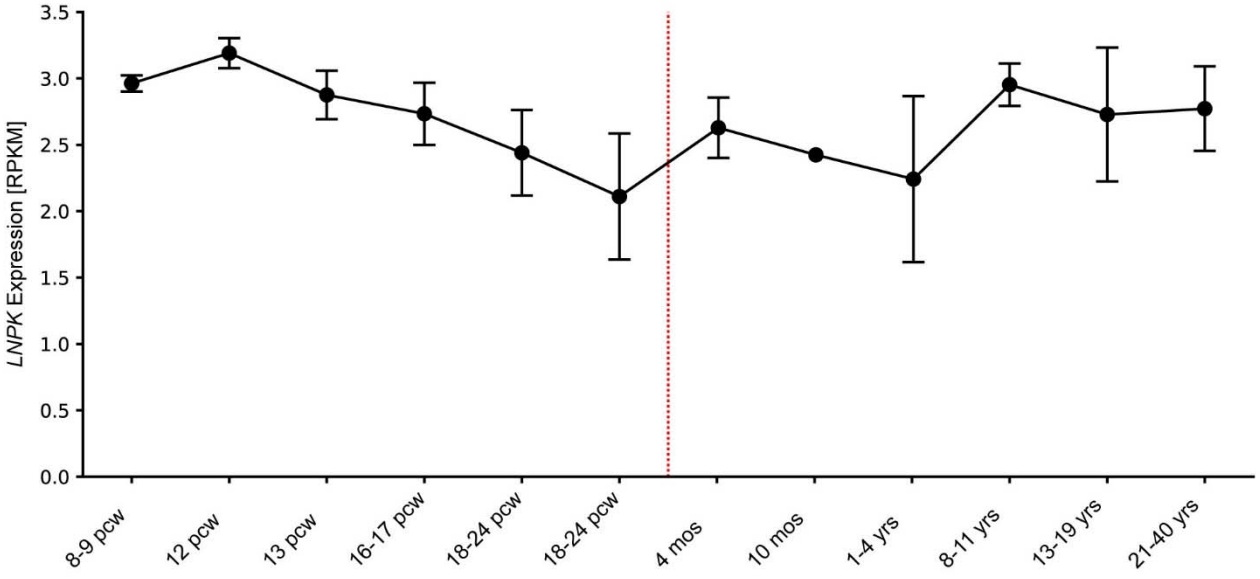

Figure S4. *LNPK* expression in the human cortical region along the developmental trajectory (BrainSpan data).

Expression analysis of *LNPK* transcripts in the developing and adult cortical regions. *LNPK* shows ubiquitous expression across all time points. Expression is shown as Reads Per Kilobase of transcript, per Million mapped reads (RPKM). Data used was derived from RNA-Sequencing data from BrainSpan.[35] Shown are mean ± SD for each time point. pcw: post-conception weeks; mos: months; yrs: years. The red line separates prenatal and postnatal time points.

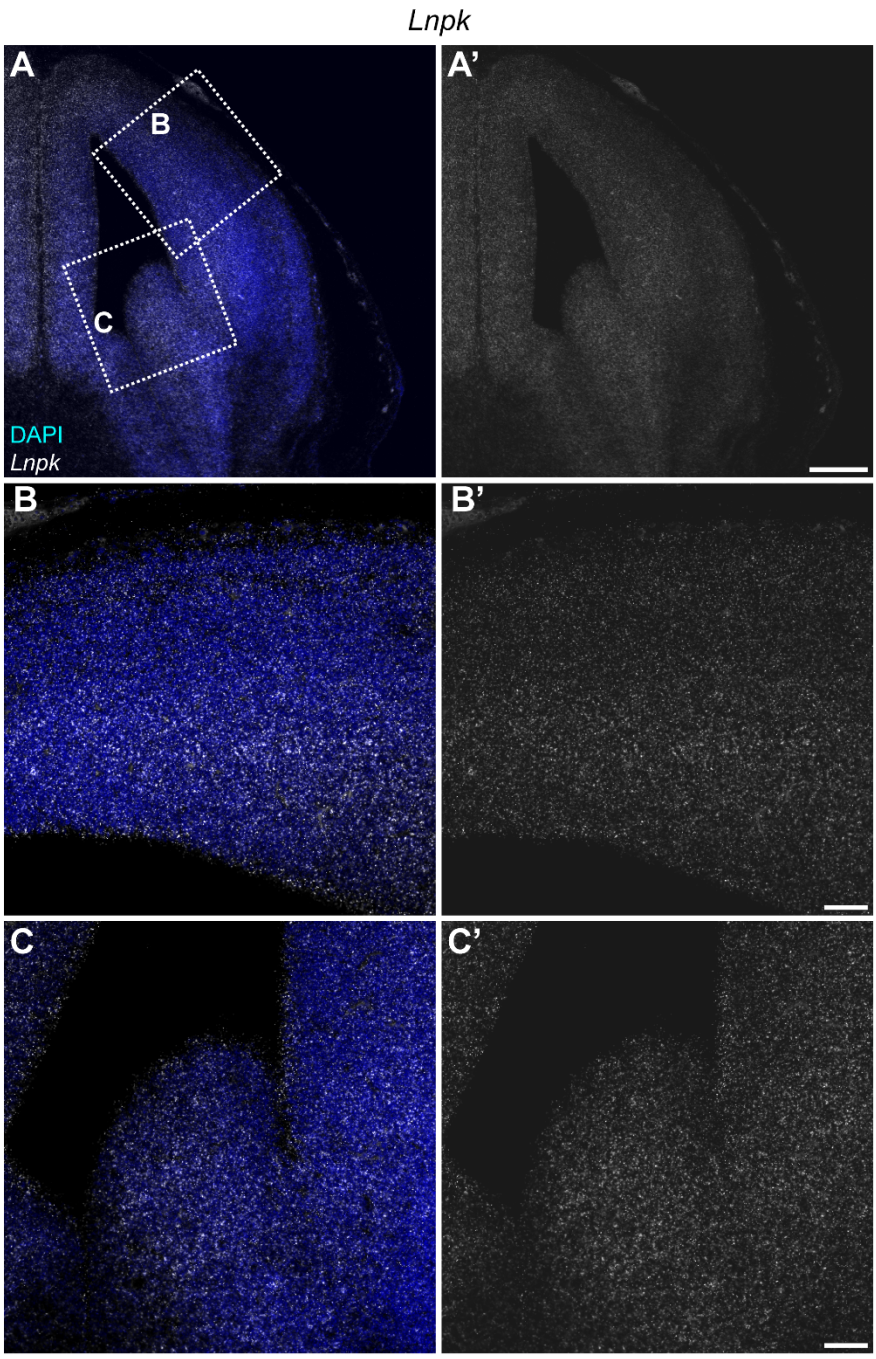

Figure S5. *Lnpk in situ* hybridization using RNAscope.

(A-C) Images of an *in situ* hybridization using RNAscope against the *Lnpk* mRNA transcript. Shown are DAPI and the *in situ* signal. A', B', and C' show *Lnpk* channel in grey scale. B and C are magnified images of the boxed regions in A for the dorsal and ventral cortex, respectively.

Note that Figure 2B was derived from the image shown in B here. *Lnpk* shows ubiquitous expression across the entire developing forebrain. Scale bars show 200 μm in A', and 50 μm in B' and C'.

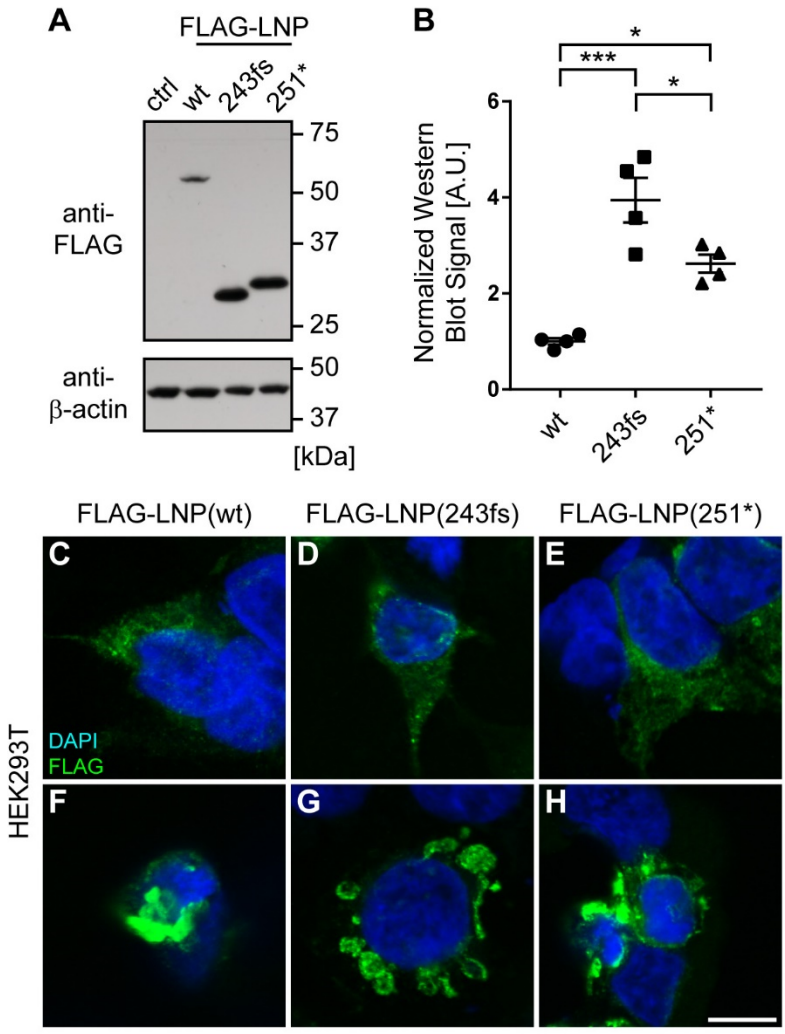

Figure S6. Truncated proteins are stable and appear to maintain correct subcellular localization when overexpressed.

(A) Western blot images probing for the FLAG-tag and β-actin in parallel blots using the same input. Shown is one example of a blot for HEK293T cell lysates following transfection with either no vector (ctrl), or a FLAG-tagged version of wild-type or mutant LNP. The two truncating mutations are abbreviated with 243fs and 251*, respectively.

(B) Quantification of the samples shown in A. FLAG signal was normalized to β-actin. Note that both truncated proteins appear to be more abundant in an overexpression situation, suggesting increased protein stability upon removal of the C-terminal domain. Shown are individual data

points, as well as the mean ± SEM. One-way ANOVA, Tukey multiple comparisons test: *P<0.05, ***P<0.001. n=3 independent experiments.

(C-E) Images for HEK293T cells overexpressing FLAG-tagged versions of wild-type or mutant LNP at moderate levels. Cells are stained with DAPI and an antibody recognizing the FLAG-tag. Subcellular localization of truncated protein resembles that of the wild-type.

(F-H) Images for HEK293T cells overexpressing FLAG-tagged versions of wild-type or mutant LNP at high levels. All variants accumulate in large vesicle-like structures that are distinct from the localization in cell expressing the constructs at moderate levels. Nevertheless, expression patterns are similar between wild-type and mutants. Scale bar shows 10 μm in H.

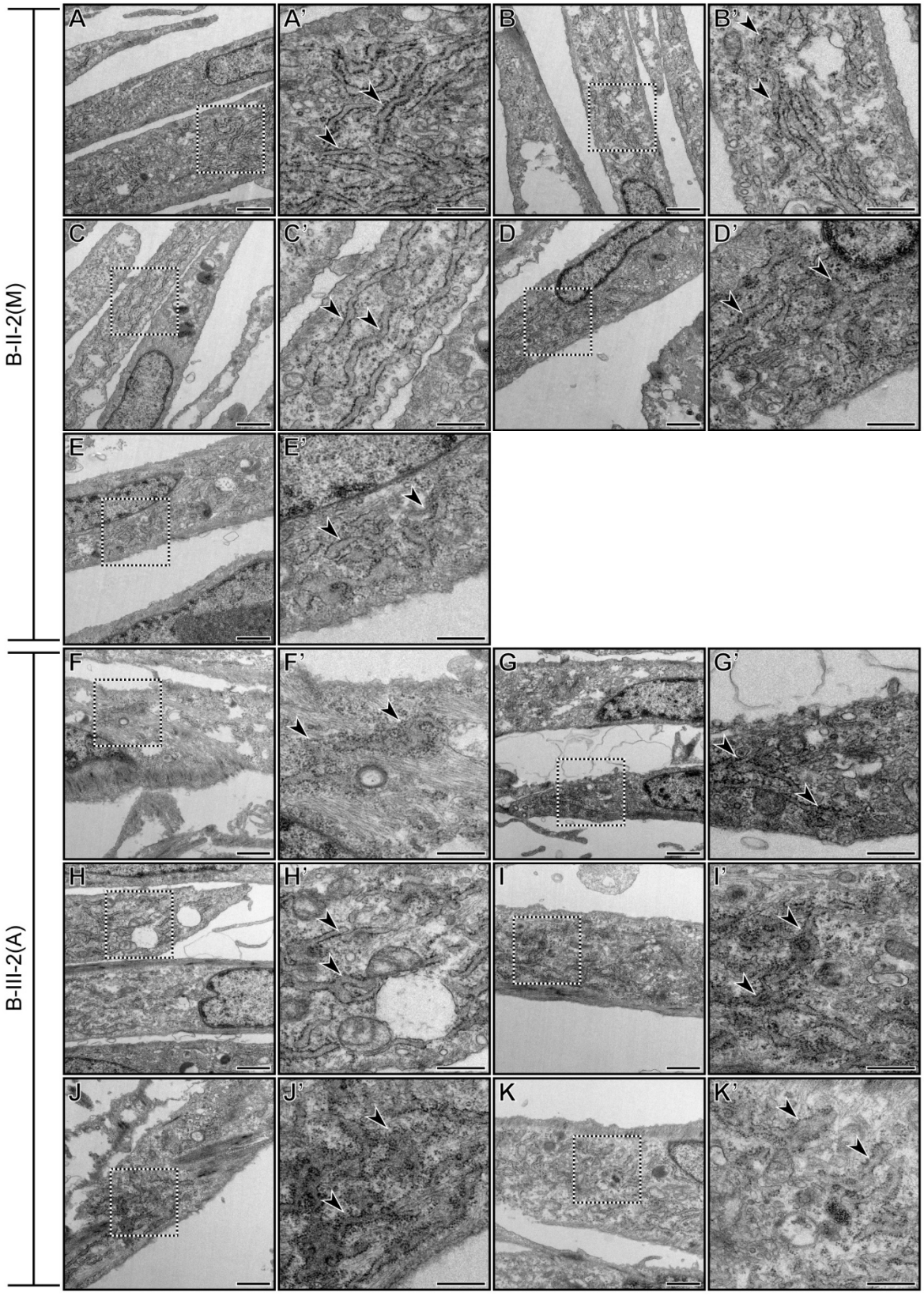
B-II-2(M)
B-III-2(A)
A
A'
B
B''
C
C'
D
D'
E
E'
F
F'
G
G'
H
H'
I
I'
J
J'
K
K'

Figure S7. Fibroblasts with a truncating mutation in *LNPK* show aberrant ER morphology.

(A-K) Series of example images for B-II-2(M) (A-E) and B-III-2(A) (F-K) fibroblasts to illustrate the aberrant ER morphology that is frequently observed in the cells derived from the affected girl. Images marked with ‘ are magnifications of the boxed region in the corresponding image. Arrowheads indicate structures identified as rough ER. Scale bars show 1 μm in A-K, and 500 nm in A’-K’.

Table S1. Mutations in *LNPK* cause various phenotypes, including corpus callosum hypoplasia, hypotonia, and epilepsy – extended clinical table.

ND: no data. SD: standard deviations (calculated using SimulConsult's measurement resources). HC: head circumference. VEP/ERG: visual evoked potential/electroretinography. EMG: electromyography. TMS: tandem mass spectrometry screening for metabolic disease.

Individual	A-III-1	A-III-2	B-III-2
Mutation (genomic)	hg19:Chr2:176804365GT>G	hg19:Chr2:176804365GT>G	hg19:Chr2:176804341G>A
Mutation (protein)	p.Pro243LeufsTer2	p.Pro243LeufsTer2	p.Arg251Ter
Mutation (cDNA)	c.726delA	c.726delA	c.751C>T
Gender	M	M	F
Origin	Egypt	Egypt	Pakistan
Consanguinity	First cousins	First cousins	First cousins
Age at diagnosis	15 y	7 y 4 mos	14 months
Weight at birth (kg)	3 kg (-0.9 SD)	2.8 (-1.2)	2.9 (-1.0)
Length at birth (cm)	51.5 cm (+0.5 SD)	50 (mean)	51 (+0.6)
HC at birth (cm)	33 cm (-1.3 SD)	34 (-0.8)	34 (-0.5)
Weight at last examination (kg), age	58 kg (16 y) (-0.2 SD)	21 (8 y 2 mos) (-1.6)	28kg (13.5 y) (-2.8)
Length at last examination (cm), age	157 cm (16 y) (-1.8 SD)	114 (8 y 2 mos) (-2.5)	139 (13.5 y) (-2.8)

HC at last examination (cm), age	53.5 cm (16 y) (-1.1 SD)	51cm (8 y 2 mos) (-1.0)	52 (13.5 y) (-1.4)
Psychomotor development			
Gross motor	Delayed	Delayed	Significant delay
Fine motor	Delayed	Delayed	Significant delay
Language	Absent	Delayed	Significant delay
Social	Delayed	Delayed	Significant delay
Regression	Progressive	Stationary	Progressive (bedridden)
Neurological findings			
Higher cognitive functions	Severe intellectual disability, no speech, autistic features, very limited social interaction, hyperactivity, inattention, dementia	Intellectual disability, few unclear words, mild autistic features, hyperactive, inattention, minimal aggressiveness	Vegetative state
Extrapyramidal symptoms	Rigidity, drooling	ND	Rigidity
Brainstem findings	No	No	No
Cerebellar deficits	No	No	Bedridden
Vision	Normal	Normal	Normal
Motor deficits	Hypertonia, only crawling	Ambulatory	Flaccid
Muscle tone	Hypotonia with rigidity	Mild hypotonia	Flaccid
Reflexes	Present	Present	Flaccid
Sensory	Normal	Normal	Not possible

Gait	Incapable	Wide based	Ataxia
Seizures			
Onset	2 y	2 y	1 y
Type(s)	Myoclonic, tonic and extension spasm	Myoclonic	Generalized tonic clonic
Most frequent type	Myoclonic	Myoclonic	Generalized tonic clonic
Frequency	Every several days	Controlled	Unknown
Treatment	Valproate, Levetiracetum, Clonazepam	Valproate, Levetiracetum	Valporate, Carbamazepine
Other systemic findings			
Immunodeficiency	No	No	Frequent infections
Musculoskeletal	Feet deviation inward	No	Scoliosis present
Skin	Normal	Hypopigmentation in groin	Normal
MRI findings			
Cerebral cortex	Normal	Normal	Normal
Corpus callosum	Hypoplasia	Hypoplasia	Hypoplasia
Brain stem	Normal	Normal	Normal
Cerebellum	Normal	Mild vermian hypoplasia	Atrophy
Other observations			
Creatine phosphokinase level	Normal	Normal	Normal
Metabolic work up	Normal	Normal	Normal

VEP/ERG	Normal	Normal	Not available
EMG	Normal	Normal	Normal
TMS	Normal	Normal	Normal
Eye	Pigmentation in sclera	Pigmentation in sclera	Normal

Table S2. Primer Sequences.

LNPK_SeqF	CACACACACACACATCCTGT
LNPK_SeqR	ATGGCCTGAAGTGGAAGTCC
LNP_F_FLAGcloning	gggGAATTCATGgactacaaggacgatgacgataagATGGGTGGATTATTTTCTCGAT
LNP_R_FLAGcloning	gggCTCGAGctaCTCTGCCGTCAAAGATTCTC
LNP_243fs_F_mut	ATAGGTCTTGCTAAAGGGGACCTGGAGGATGAAG
LNP_243fs_R_mut	CTTCATCCTCCAGGTCCCCTTTAGCAAGACCTAT
LNP_251*_F_mut	CAAAGCACCTCGTTCTCAGGGGAGAATAGGTCTTG
LNP_251*_R_mut	CAAGACCTATTCTCCCCTGAGAACGAGGTGCTTTG
mmLnpk_qPCR_F	AAGCCAGCTCATTGAAGAC
mmLnpk_qPCR_F	TGTCATCTCTCTGCTCAGTAC
hsLNPK_qPCR_F	GTCATCTGTCTGCTCTGTATTATC
hsLNPK_qPCR_R	TGCTTTCATCAGACAACCAG
mmPgk1_qPCR_F	AAAGTCAGCCATGTGAGCACT
mmPgk1_qPCR_R	ACTTAGGAGCACAGGAACCAAA
mmTfrc_qPCR_2F	TCGCTTATATTGGGCAGACC
mmTfrc_qPCR_2R	ATCCAGCCTCACGAGGAGT
mmHprt_qPCR_3F	GAACCAGGTTATGACCTAGATTTGTT
mmHprt_qPCR_3R	CAAGTCTTTCAGTCCTGTCCATAAT
hsHPRT_qPCR_F	TGACACTGGCAAAACAATGCA
hsHPRT_qPCR_R	GGTCCTTTTCACCAGCAAGCT
hsPGK1_qPCR_F	ATGGATGAGGTGGTGAAAGC
hsPGK1_qPCR_R	CAGTGCTCACATGGCTGACT
hsTBP_qPCR_F	TGCACAGGAGCCAAGAGTGAA
hsTBP_qPCR_R	CACATCACAGCTCCCCACCA

Supplemental Materials and Methods

Recruitment. The procedures followed for recruitment and data collection were in accordance with the ethical standards of the responsible committee on human experimentation at the respective, participating institute and proper informed consent was obtained.

DNA extraction and whole exome sequencing. DNA was extracted on an Autopure LS instrument (Qiagen, Valencia, CA) with Autopure chemistry according to the manufacturer's instructions. Samples of the three affected individuals and the two unaffected parents were subjected to Agilent Sure-Select Human All Exon v2.0 (44Mb baited target) library preparation sequencing on an Illumina HiSeq 2000 with v2 chemistry (Read Length: 151). The accession number for these data is dbGAP: phs000288.v1.p1.

Computational analysis. Variant calling and filtering were performed according to our previously described whole exome sequencing pipeline.[1] Variants were filtered if not present in both affected in Family A. For both families, they were filtered if the minor allele frequency (MAF) was >1:10,000, or if they yielded PolyPhen-2 prediction scores of <0.9 or GERP score <4.5. Calls were also checked with MutationTaster and homozygosity was confirmed using the online tool HomozygosityMapper.[2-4]

Sanger sequencing. Sanger sequencing of PCR products covering exon 10 of *LNPK* was performed using standard procedures (LNPK_SeqF/R; Table S2). Individual allele sequences were obtained by TOPO TA cloning (Life Technologies, 450641) and colony PCR according to the manufacturer's instructions and standard protocols. Sequencing tracks were visualized with SnapGene Viewer (SnapGene).

Cell culture experiments and immunocytochemistry. Cell culture maintenance and transfection was described previously.[5] Fibroblasts (obtained from dermal biopsies and ATCC for the control) and NPCs were generated and cultured as described before.[6] N-terminally FLAG-tagged LNP was cloned using the sequence in the Lnp1-GFP vector, a kind gift of the Ferro-Novick laboratory, into the pcDNA3.1+ vector (LNP_F/R_FLAGcloning; Table S2).[7] The mutations were introduced using the Quikchange Lightning Site-Directed Mutagenesis Kit according to the manufacturer's instructions (Agilent Technologies, 210518; LNP_243fs/251*_F/R_Q5Mut; Table S2). Constructs were transfected the day before fixation and staining. Transfected cells, fibroblasts, and NPCs were fixed in 4% paraformaldehyde and immunocytochemistry was performed using standard protocols. The employed antibodies were: anti-DDDDK tag (Abcam, ab1162, 1:1000), anti-Lunapark (Sigma-Aldrich, HPA014205, 1:200), anti-SOX2 (Santa Cruz, sc-17320, 1:200), and anti-TUBB3 (Tuj1, BioLegend, 801202, 1:1000). Cells were counterstained with DAPI (Thermo Fisher, D1306, 1:2000). Images were acquired with a Leica SP5 microscope and processed with ImageJ/Fiji.[8; 9]

Quantitative RT-PCR. RNA extraction, cDNA synthesis, and qPCR were performed as described previously.[10] Primers employed are listed in Table S2.

RNAscope in situ *hybridization*. *In situ* hybridization was performed using RNAscope technology (Advanced Cell Diagnostics, 322000) with custom probes against *Lnpk* (Advanced Cell Diagnostics).[11] Images were acquired with a Leica SP5 microscope and processed with ImageJ/Fiji.

Western blot. Cells were lysed with ice-cold RIPA buffer and assessed by Western blot using standard protocols. Primary antibodies used were anti-beta-Actin (Santa Cruz, sc-47778, 1:2000), anti-FLAG-tag (Sigma, F3165, 1:1000), and anti-Lunapark (Sigma-Aldrich,

HPA014205, 1:1000). Western blot signal intensity (area of peaks) was analyzed using ImageJ/Fiji and normalized to the loading control.

Transmission electron microscopy and analysis. Fibroblasts were immersed in modified Karnovsky's fixative (2% glutaraldehyde in 0.1M sodium cacodylate buffer, pH 7.4) for 30 minutes at room temperature, scraped and pelleted and resuspended in fresh fixative again for at least 4 hours at 4°C, postfixed in 1% osmium tetroxide in 0.1M cacodylate buffer for 1 hour and stained *en bloc* in 2% uranyl acetate for 1 hour. Pellets were dehydrated in ethanol, embedded in Durcupan epoxy resin (Sigma-Aldrich), sectioned at 50 to 60 nm on a Leica UCT ultramicrotome, and picked up on 300 mesh copper grids. Sections were stained with 2% uranyl acetate for 5 minutes and Sato's lead stain for 1 minute. Grids were viewed using a JEOL 1200EX II (JEOL, Peabody, MA) transmission electron microscope and photographed using a Gatan digital camera (Gatan, Pleasanton, CA). EM images were automatically anonymized and analyzed by a person blind to the conditions and the expected phenotypes. Unbiased stereology was achieved using ImageJ/Fiji by overlaying a grid with an area of 100000 pixels^2 per point on images with an image as shown in Figure 4B (4090x4090 pixels).[12] Each grid point was assessed in order to determine whether it was overlaying an intact cell, and whether it was overlaying rough ER or not. The coordinates were then imported using Python (3.64) (Python Software Foundation, https://www.python.org/) with Pandas (0.22.0).[13] These data were then directly used for the analysis of fractional abundance ([points within rough ER]/[all points within cellular area]). For grey value analysis, images were imported as NumPy (1.13.3) matrices using Scikit-image (0.13.0).[14; 15] In order to reduce variability due to single pixel measurements, average grey values were obtained by averaging the grey values of a square of 5x5 pixels, centered around the coordinates of each point. In addition all values were normalized for the varying background intensities; these were obtained by measuring 5 points representing

background intensities from the four corners and the middle of the image (as much spaced apart as possible) and using squares of 21x21pixels.

GTEx and BrainSpan. Data was obtained from the GTEx and BrainSpan (© 2010 BrainSpan Atlas of the Developing Human Brain. Available from brainspan.org) portals and processed using Python (3.64) with Pandas (0.22.0).

Visualization and statistical analysis. Statistical analysis was done as indicated in figure legends using GraphPad Prism 7. Visualization of data was performed using GraphPad Prism 7 (Figures 2, 3, and S6) or using Python (3.64) with Seaborn (0.8.1).[16]

Supplementary References

1. Dixon-Salazar, T.J., Silhavy, J.L., Udpa, N., Schroth, J., Bielas, S., Schaffer, A.E., Olvera, J., Bafna, V., Zaki, M.S., Abdel-Salam, G.H., et al. (2012). Exome sequencing can improve diagnosis and alter patient management. Sci Transl Med 4, 138ra178.
2. Seelow, D., and Schuelke, M. (2012). HomozygosityMapper2012--bridging the gap between homozygosity mapping and deep sequencing. Nucleic Acids Res 40, W516-520.
3. Seelow, D., Schuelke, M., Hildebrandt, F., and Nurnberg, P. (2009). HomozygosityMapper--an interactive approach to homozygosity mapping. Nucleic Acids Res 37, W593-599.
4. Schwarz, J.M., Rodelsperger, C., Schuelke, M., and Seelow, D. (2010). MutationTaster evaluates disease-causing potential of sequence alterations. Nat Methods 7, 575-576.
5. Breuss, M.W., Nguyen, T., Srivatsan, A., Leca, I., Tian, G., Fritz, T., Hansen, A.H., Musaev, D., McEvoy-Venneri, J., James, K.N., et al. (2017). Uner Tan syndrome caused by a homozygous TUBB2B mutation affecting microtubule stability. Hum Mol Genet 26, 258-269.
6. Akizu, N., Cantagrel, V., Schroth, J., Cai, N., Vaux, K., McCloskey, D., Naviaux, R.K., Van Vleet, J., Fenstermaker, A.G., Silhavy, J.L., et al. (2013). AMPD2 regulates GTP synthesis and is mutated in a potentially treatable neurodegenerative brainstem disorder. Cell 154, 505-517.
7. Chen, S., Desai, T., McNew, J.A., Gerard, P., Novick, P.J., and Ferro-Novick, S. (2015). Lunapark stabilizes nascent three-way junctions in the endoplasmic reticulum. Proc Natl Acad Sci 112, 418-423.
8. Rueden, C.T., Schindelin, J., Hiner, M.C., DeZonia, B.E., Walter, A.E., Arena, E.T., and Eliceiri, K.W. (2017). ImageJ2: ImageJ for the next generation of scientific image data. BMC Bioinformatics 18, 529.
9. Schindelin, J., Arganda-Carreras, I., Frise, E., Kaynig, V., Longair, M., Pietzsch, T., Preibisch, S., Rueden, C., Saalfeld, S., Schmid, B., et al. (2012). Fiji: an open-source platform for biological-image analysis. Nat Methods 9, 676-682.
10. Breuss, M., Heng, J., Poirier, K., Tian, G., Jaglin, X., Qu, Z., Braun, A., Gstrein, T., Ngo, L., Haas, M., et al. (2012). Mutations in the β-Tubulin Gene TUBB5 Cause Microcephaly with Structural Brain Abnormalities. Cell Rep 2, 1554-1562.
11. Feng, J., Xian, Q., Guan, T., Hu, J., Wang, M., Huang, Y., So, K.F., Evans, S.M., Chai, G., Goffinet, A.M., et al. (2016). Celsr3 and Fzd3 Organize a Pioneer Neuron Scaffold to Steer Growing Thalamocortical Axons. Cereb Cortex 26, 3323-3334.
12. Howard, V., and Reed, M. (2004). Unbiased stereology: three-dimensional measurement in microscopy.(Garland Science).
13. McKinney, W. (2010). Data Structures for Statistical Computing in Python. In Proceedings of the 9th Python in Science Conference, S.v.d. Walt and J. Millman, eds., pp 51-56.
14. Oliphant, T.E. (2006). A guide to NumPy.(Trelgol Publishing USA).
15. van der Walt, S., Schonberger, J.L., Nunez-Iglesias, J., Boulogne, F., Warner, J.D., Yager, N., Gouillart, E., Yu, T., and scikit-image, c. (2014). scikit-image: image processing in Python. PeerJ 2, e453.
16. Waskom, M., Botvinnik, O., O?Kane, D., Hobson, P., Lukauskas, S., Gemperline, D.C., Augspurger, T., Halchenko, Y., Cole, J.B., Warmenhoven, J., et al. (2017). mwaskom/seaborn: v0.8.1 (September 2017). In. (